International Journal of Heat and Mass Transfer 52 (2009) 5496–5511

Contents lists available at ScienceDirect

International Journal of Heat and Mass Transfer

journal homepage: www.elsevier.com/locate/ijhmt

Numerical simulation of turbulent flow in a Ranque–Hilsch vortex tube

A. Secchiaroli *, R. Ricci, S. Montelpare, V. D'Alessandro

Università Politecnica delle Marche, Dipartimento di Energetica, Via Brecce Bianche, 60100 Ancona, Italy

ARTICLE INFO

Article history:
Received 19 September 2008
Accepted 30 May 2009
Available online 11 August 2009

Keywords:
Ranque–Hilsch vortex tube
Compressible flow numerical simulation
Turbulence models
Reynolds stress models
LES

ABSTRACT

The present work is about numerical simulations of the internal flow in a commercial model of a Ranque–Hilsch vortex tube (RHVT) operating in jet impingement. Simulation of the turbulent, compressible, high swirling flow was performed by both RANS and LES techniques. The effect of different turbulence closure models have been tested in RANS simulations using a first order closure RNG k–ε and, for the first time in this kind of flow, a second order RSM (Reynolds Stress differential Model) closure. RANS computations have been executed on an axis-symmetric two-dimensional mesh and results have been compared with LES ones, obtained over a three-dimensional computational grid. Smagorinsky sub-grid scale model was used in LES. All the calculations were performed using FLUENT™ 6.3.26. The use of a common code for the different simulations allowed the comparison of the performances of the different techniques and turbulence models, avoiding the introduction of other variables.

In all the simulations performed, consistency with the real commercial vortex tube model in jet impingement operation has been followed by substituting an axial hot computational exit to the usual radial one. Comparison of the results between RANS simulations performed on both a traditional radial hot outlet computational domain and one with an axial hot outlet, demonstrates the suitability of the computational model adopted in this work, closer to the real geometry of the device, particularly in RANS RSM simulations. Results in different sections of the tube show significant differences in the velocity profiles, temperature profiles and secondary vortex structures, varying turbulence model.

The accurate numerical simulation of the flow in a RHVT, resulting in an improved prediction capability of the kinematic and thermal properties of outgoing jets, could allow a correct estimation of the cooling performance of this device in jet impingement operation.

1. Introduction

The Ranque–Hilsch vortex tube (RHVT) is a simple device in which a compressed gas flow is split into two low pressure flows whose temperatures are, respectively, higher and lower than the one of the inlet flow. This effect, called the Ranque–Hilsch effect or "thermal separation", is merely a fluid dynamic process as it takes place in a device with no moving parts.

The RHVT consists of a circular tube with an inlet orifice, where compressed gas flows tangentially through several nozzles, azimuthally arranged. The high pressure flow affected from very strong swirling motion is split into two streams of different temperatures: the hotter one spiraling in touch with the wall in the outer zone of the tube, the colder one spiraling in the opposite direction close around the central axis (Fig. 1). The hot and cold gas streams leave the device through two axial outlet orifices that can be arranged either both on the same side of the tube (uni-flow vortex tube) or on the opposite sides of the tube (counter-flow vortex tube). The mass flow rate is regulated by a cone-shaped control valve, placed near the hot exit. This valve can vary the mass flow rate leaving the hot exit influencing the temperature of the gas leaving the device. The commercial RHVT modeled in this paper is a counter-flow Exair® 25 scfm, as in [1], supplied by compressed air.

The RHVT is today used in several industrial applications like separating gas mixtures, liquefying gases, purifying and dehydrating two-phase mixtures, cooling tools in operation, cooling cabinets of electronic devices, separating particle in gas streams, etc. It is well suited for these applications because it allows an accurate temperature control, it is light, it does not require any maintenance, it is easy to use and it can work with different gases. Thermal separation effect is reported to work supplying RHVT with high pressure liquids too [2], although in this case, the cold stream never reaches as a low temperature as the one of the inlet stream because of the important role played by fluid compressibility in the cooling process of the internal stream.

Many efforts to explain the thermal separation phenomenon have been made in the past, based on theoretical, numerical and experimental analysis. First pioneer works were due to Ranque in 1932, and Hilsch in 1947. Ranque explained the phenomenon by

* Corresponding author. Tel.: +39 0712204359; fax: +39 0712204770.
E-mail addresses: a.secchiaroli@univpm.it, alessiosecchiaroli@gmail.com (A. Secchiaroli).

0017-9310/$ - see front matter © 2009 Elsevier Ltd. All rights reserved.
doi:10.1016/j.ijheatmasstransfer.2009.05.031

Nomenclature

u_i,u_j,u_k	velocity vector components (m/s)
E	total internal energy per unit mass (J/kg)
e	cold fraction value
x_i,x_j,x_k	position vector components (m)
R	universal gas constant = 8.314 (J/K mol)
h	enthalpy per unit mass (J/kg)
p	pressure (Pa)
T	temperature (K)
k	turbulent kinetic energy (m^2/s^2)
a	speed of sound (m/s)
S_{ij}	strain rate tensor ij-component (s^{-1})
M	Mach number
c_P	constant pressure specific heat (kJ/kg K)
Pr	Prandt number
GCI	grid convergence index
t	time (s)
G	generic filter function for LES
C_R	Smagorinsky's constant
E_p	Asymptotic range verification parameter (methods of order p) $\approx \mathrm{GCI}/1.25 \cdot \Delta x^p$

Greek symbols

λ	thermal conductivity (W/mK)
μ	dynamic viscosity (Pa s)
δ_{ij}	Kronecker symbol
ϕ_j	conductive heat flux (W/m^2)
Δ_x	grid spacing (m)
ρ	density (kg/m^3)
ε	turbulent dissipation rate (m^3/s^2)
$\overline{\Delta}$	filter length in LESs (m)

Superscript

$\bar{f}$	averaged variable in time or space
f'	turbulent fluctuating variable around averaged value
$\tilde{f}$	Favre's averaged variable in time or space
f''	Turbulent fluctuating variable around Favre's averaged value
d	deviatoric
i	isotropic
t	turbulent
v	viscous
0	stagnation value

Subscripts

SGS	sub-grid scale
η	Kolmogorov length scale
h	hot outlet
c	cold outlet

means of adiabatic expansion in the central core of the fluid flow (cooling flow) and adiabatic compression of peripheral flow (heating flow). Hilsch later introduced the effect of the internal friction between the gas layers, improving Ranque's results. These models were rejected by Fulton on account of the process not being fully adiabatic. Further researches, in the following years, showed the role of the friction and of the turbulence mixing in the thermal separation phenomenon. Moreover, damping of acoustic streaming along the axis of the tube was involved in the explanation of the RHVT characteristics too, by Kurosaka [3]. One of the most important contribution in determining the flow pattern inside a vortex tube is due to Ahlborn and co-workers [4,5] who proposed the "secondary circulation model", based on his experimental results. He showed the existence of a secondary circulation by showing that the mass flow rate, through a cross-section of the tube, moving toward the cold end was larger than the cold outflow mass. This secondary flow (Fig. 2) can be considered as the operating fluid in a classic thermodynamic refrigerant cycle, because two almost-adiabatic transformation (compression/expansion) and two heat exchanges operate on it during the circulation inside the RHVT. A description of the principal explanation efforts of the Ranque–Hilsch effect can be found in Gao [6,7], who developed a

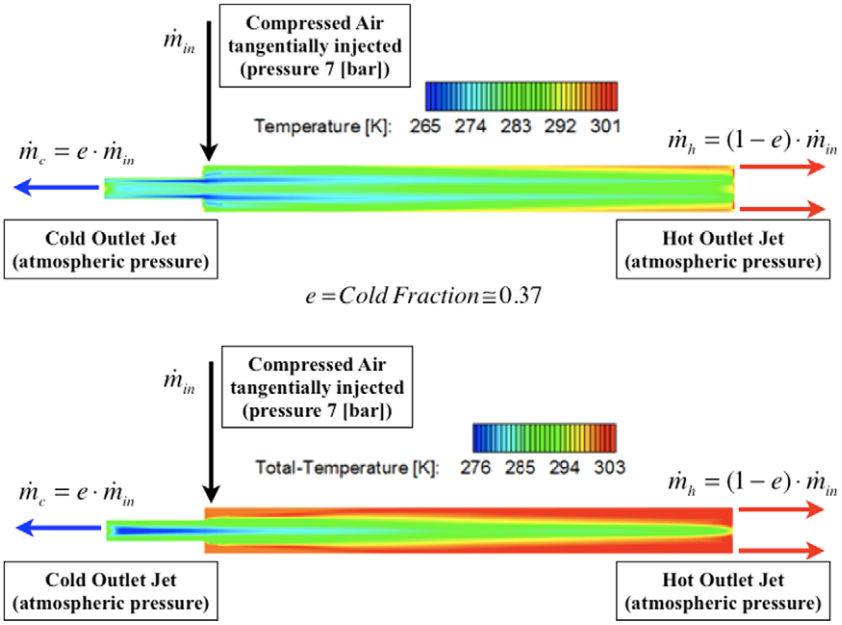

Fig. 1. Static and total temperature map in a LES (time-averaged results) with Smagorinsky sub-grid model.

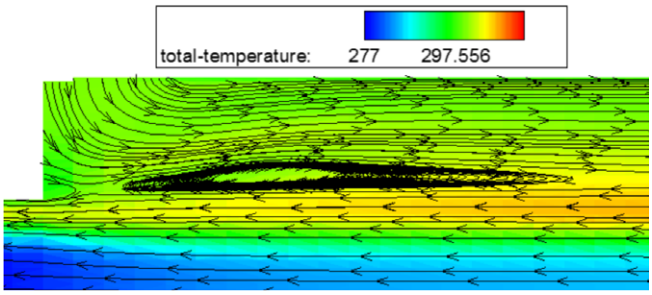

Fig. 2. Visualization of secondary circulation in a RANS simulation with RSM closure model (inlet section).

modified version of the Ahlborn's theory. Assuming a tangential velocity distribution along the radius in the inlet section of the vortex chamber in the shape of a Rankine vortex, and considering compressible the inlet flow, he developed an empirical model to predict the thermal separation which resulted more realistic than the Ahlborn's one.

A numerical simulation of the internal flow field was performed in a recent work using the RANS approach on a computational model with an axial hot outlet [8]. It showed the relative influence of both mechanical work (due to swirl and axial velocity gradient) and heat transfer (due to static temperature difference between fluid layers) on the thermal separation process. Numerical results stated that the angular velocity gradient between the inner faster layers and the peripheral slower ones set-up an energy transfer due to the action of viscous shear. As a result the cooling of the core flow and the heating of the peripheral flow takes place. It is worthwhile noting that the counter acting energy transfer due to viscous shear and produced by the axial velocity gradient has a negligible effect on the thermal separation. Moreover, the effect of the heat transfer due to the static temperature difference is relevant only in the section of the tube near the inlet.

During the past few years the research studies on RHVT, have been separated in to two main groups: the first one dedicated to experimental works, aimed to explain the phenomenon by means of data obtained in test bed and designed for vortex tube performance evaluation; the second one related to analytical and numerical studies of the internal flow field, attempting to determine its implication in thermal separation. A complete review of theoretical, experimental and numerical works about vortex tubes can be found in [9]. The experimental study of the internal flow field in a RHVT is a challenging task. On one hand, conventional velocity measurements techniques in fluids (Pitot tube, HWA, etc.) are by far too intrusive and the small diameter of the tube, along with the high velocity of the flow, makes them inaccurate. On the other hand even non-intrusive optical measurement methods, which rely on the use of seeding particles released in the flow, are unable to provide accurate informations due to high centrifugal acceleration. The observations above clearly explain why experimental researches are mainly intended to measure the performances variations related to the modification of design parameters such as mass cold fraction or components geometry (i.e. nozzles characteristics, control valve shape, etc.). As a matter of fact tests performed by inserting a vortex tube in a closed circuit hardly provide useful informations about the internal fluid dynamic of the RHVT operating in jet impingement conditions and the measures of the mass flow rate, the pressure and the temperature at the inlet and outlets in test bed might result significantly different from the ones observed in jet impingement cooling. Another thing to take into account when considering these kinds of tests is the necessity of replacing the cone-shaped valve with a regulated one placed along the pipeline. The presence of this valve might affect the functional length of the RHVT which is directly related to the performances of the tube [6]. From what said follows that data obtained by closed circuit test bed cannot be compared with numerical simulation intended to reproduce internal fluid dynamic behavior in jet impingement operation. A comparison between numerical simulation and experimental data is available in [10] but in this case, the set-up of the experimental apparatus forces the hot exit to be radial rather than axial, resulting in an unrealistic condition for jet impingement applications. As a consequence, these experiments are not reliable enough when predicting, for example, flow patterns of outgoing jets that would be useful data when studying jet impingement cooling applications of this device. In such conditions an accurate numerical analysis would be the only effective way to obtain information about velocity, pressure and temperature fields in the simulation domain as well as at the outlets. These data might be experimentally verified, in authors' opinion, by using PIV measurements in the free jet near the exits or by using internal measurements in a larger RHVT once investigated the scaling of velocity and temperature fields with vortex tube dimensions by other CFD analysis.

On the grounds of the above mentioned observations stems the present work whose aim is the development of an accurate numerical simulation of the flow field and its physical characteristics inside a commercial RHVT. Turbulence was analysed, by means of RANS and LESs simulations using the commercial CFD code FLUENT™ 6.3.26. In RANS simulations several turbulence closure models were tested, trying to improve the numerical code prediction capability in swirling compressible turbulent flows.

In particular, RSM (Reynolds Stress differential Model) in RANS simulations were used successfully for the first time in a vortex tube numerical model. In addition, LESs of an RHVT flow were performed using a Smagorinsky sub-grid closure. The use of a computational model with hot axial outflow (for the first time in large eddy simulations), very close to real geometry of the commercial vortex tube was compared to the use of the more common radial hot outlet one. Grid independence procedure, evaluated by means of Richardson extrapolation technique was used for all the simulations performed.

2. Vortex tube model description

2.1. Geometrical domain

Ranque–Hilsch vortex tube used in this work is a commercial counter-flow model produced by Exair Company and it is the same model used in [1]; a picture with the dimensions of this device is represented in Fig. 3. Although the RHVT has no moving parts and its components are very simple, the thermo-fluid dynamic behavior is strongly influenced by its geometry. A solid CAD model of each part of the device has been developed and geometrical features of the RHVT have been completely investigated in order to have a correct understanding of the flow boundary conditions as well as to operate some simplifications in the computational domain. Results of the solid modelling along with all the components are presented in Fig. 4. The computational model was simplified in two sections: inlet section and hot exit section. In fact, the vortex tube used in this study has a radial inlet which in turn needs a particular component called "generator", which is used to transform the radial air motion into a tangential one. The generator is equipped with a series of nozzles circumferentially arranged in the vortex chamber that allow the flow stream to arrive with high tangential velocity in the vortex tube core (Fig. 5). The inlet of the computational model is obtained, as in other works [1], imposing that the value of the mass flow rate is distributed on a portion of the cylindrical surface of the vortex tube. As a consequence, at

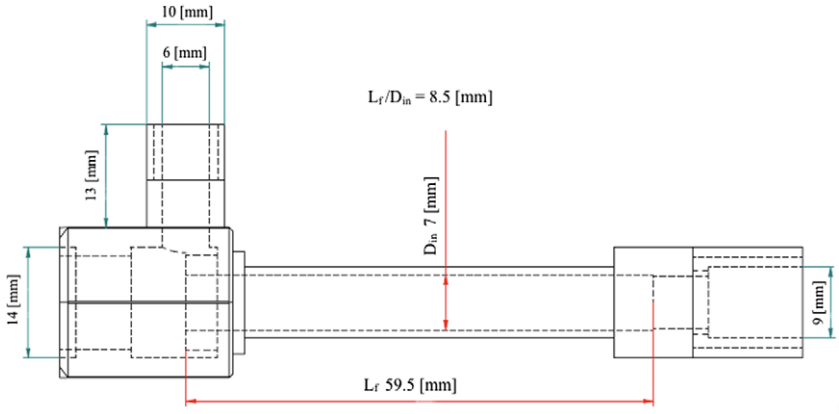

Fig. 3. Picture of vortex tube used in simulations and its dimensions.

the cylindrical inlet surface whose dimensions are listed in Table 1 corresponds a uniform distributed mass flow rate of 3.23×10^{-3} kg/s with the inlet velocity field defined in Table 4. Cold fraction value (i.e. the ratio between cold and inlet mass flow) is about 0.37.

The RHVT analysed is equipped with a control valve, placed at the hot exit that is able to reduce the mass flow rate leaving the hot side of the tube. This valve regulates the cold fraction value increasing the pressure near the hot exit. It is worth noting that its position influences the motion configuration in all the tube. In fact, large value of the outflow area (i.e. low value of the cold fraction) causes the pressure to drop at the cold exit which in turn generates a local back flow as reported in [1]. This component presents a complex geometry as showed in Fig. 5. Its cone-shaped surface leaves an annular gap exit between the valve external surface and the tube internal surface that has been used as computational outlet.

According to the literature numerical simulations of the flow in this kind of devices are usually performed considering a radial hot outlet that is less representative of a jet impingement operating condition. In [10] a computational model with radial hot outlet coupled with axial inlet was used for numerical stability reasons; this simplification was found unnecessary in this work. Hence, few numerical studies performed on a model with axial hot exit exist [8,11–13] and only RANS simulations are presented in them. Anyway, a comparison performed between RANS simulations results obtained using an axial computational hot outlet and a radial computational hot outlet, showed little differences in the predictions, as reported in Section 4.

In conclusion, the main simplifications introduced into geometrical model of the RHVT involves the inflow and hot outflow sections: inlet section was modified following Skye et al. [1], while outlet hot section was represented as an axial outflow in the computational domain.

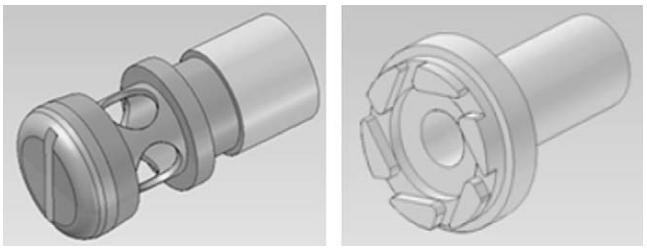

Fig. 5. Sketches of control valve (right) and generator (left).

2.2. Computational model

Different computational grids were designed for numerical simulation: RANS simulations were performed over axis-symmetric grid, while a complete three-dimensional grid was used for LESs. In particular structured Cartesian cells were used in axial-symmetric simulations, with near wall refinement, performed

Table 1
Flow conditions at the computational inlet.

Parameter	Value
Mass flow inlet $\dot{m}$ (kg/s)	3.23E−3
Inlet surface A (m^2)	4.19E−5
Inlet surface axial extension L (m)	0.002
RHVT diameter D (m)	0.007

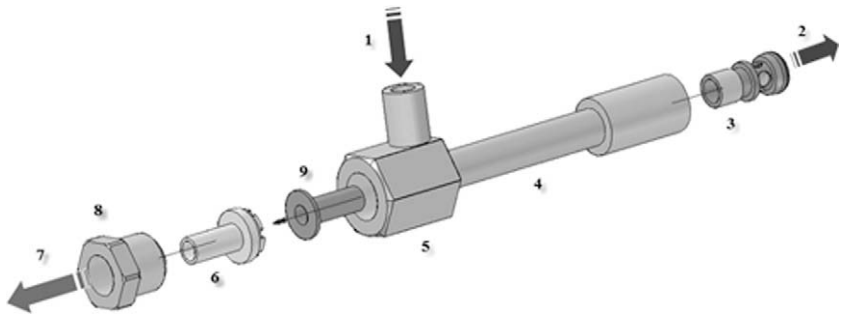

Fig. 4. Components of commercial vortex tube: 1 – air inlet; 2 – hot exit; 3 – control valve; 4 – main body; 5 – vortex chamber; 6 – generator; 7 – cold exit; 8 – threaded ring nut; and 9 – brass inset.

Table 2
RANS grids features.

Grid identification	Number of cells	ΔT^0_{hc} (K)	ΔT^0_{hc} (% error)	GCI (%)	E_P
RANS1	5000	27.6			
RANS2	2500	25	9.4	4	8.6×10^{-13}
RANS3	2055	22.6	18	4	1.5×10^{-12}
RANS4	1212	20	27.2	1.2	2.2×10^{-12}

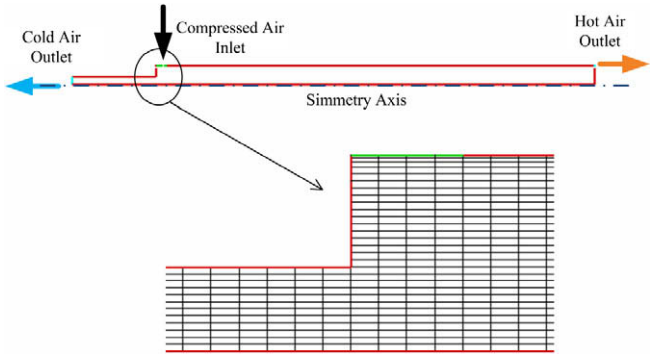

Fig. 6. Computational grid used in RANS simulations.

using standard wall-functions. A grid independence procedure was implemented by means of Richardson extrapolation technique over grids with different numbers of cells. The characteristics of the grids used in RANS simulations are listed in Table 2 and a grid sketch is presented in Fig. 6. Following Behera et al. [13], mean total temperature difference between hot and cold exit ΔT^0_{hc}, calculated in the simulation, was chosen as the most sensible physical parameter to grid spacing Δx. As can be seen from Table 2 there is very little variation in ΔT^0_{hc} when increasing the number of cells from 2500 to 5000 (9%), hence there is no such advantage in increasing the number of cells beyond this value. From the values of this parameter it follows that the grid convergence index (GCI [14]) can be obtained for different grids (Table 2). GCI represents an estimation of the discretization error between numerical solution, calculated over finer grid and numerical solutions calculated over coarser ones. Since GCI values are almost constant grid independence condition was obtained. The achieving of the asymptotic range for the discretization method order used (second order) was verified too, determining the approximate constancy of E_P parameter, as established in [14]. Grids used in LES were obtained dividing the domain volume into 36 sub-volumes to get a better control of cells skewness and dimension. Central core of the vortex tube was meshed with unstructured elements, while mesh in the external part was a structured curvilinear grid; moreover axial refinements were performed at the inlet section and at the hot exit. This way, three-dimensional model were composed of about 199,000 elements with a maximum volume of 3.03×10^{-11} m^3. A sketch of this grid is represented in Fig. 7. Coarser grids were developed to perform grid independence analysis; RANS simulations and results are listed in Table 3. In this latter case, further refinements are not useful as variation in ΔT^0_{hc} is very small when increasing number of cells from 114,611 to 198,816 (0.1%); asymptotic range is probably within reach of the LES1 and LES2 grids. Mean values of total temperature difference in LESs are lower than in RANS simulations, due to the back flow region at the cold exit predicted by the formers. Furthermore, a different type of grid for LES was tested with different shape and size of core cells; the central core was meshed with a structured mesh; the total number of cells was more than 267,000 with a maximum cell volume of 2.71×10^{-11} m^3 allowing a better symmetry of the cells in radial direction: a sketch of this mesh is depicted in Fig. 8.

3. Flow mathematical model

3.1. Governing equations

Numerical simulation of flow inside a Ranque–Hilsch vortex tube is a very difficult and challenging task, as it deals with dynamic behavior prediction of a high swirling, unsteady, compressible turbulent flow. Moreover, strong temperature gradients arise in a vortex tube either in the axial than in the radial direction; hence, the dynamic problem is strongly coupled with the thermal one. Due to its characteristics, mathematical modelling of the flow requires particular care in establishing the governing equations, in setting the solution techniques and in selecting the turbulence closure models. As a consequence of the relevance of the thermal gradients (separation effect) and of the flow compressibility, the continuity and Navier–Stokes equations are completed using the energy equation and the gas equation of state. Thermo-physical properties of the air are assumed to be varying with the temperature as a third order polynomial function. The complete set of governing equations is represented in (1)–(6) in which, gravity effects are excluded, stress tensor is related to strain rate one by constitutive relations for Newtonian fluids, and thermal flux vector is expressed by the Fourier's postulate. These equations are solved numerically by the

Table 3
LES grids features.

Grid Identification	Number of cells	ΔT^0_{hc} (K)	ΔT^0_{hc} (% error)	GCI (%)	E_P
LES1	198,816	14.3			
LES2	114,616	14.2	0.1	0.05	2.9×10^{-14}
LES3	102,240	11.4	19	10.5	6.6×10^{-12}
LES4	60,210	10.9	23	3.5	6.5×10^{-12}

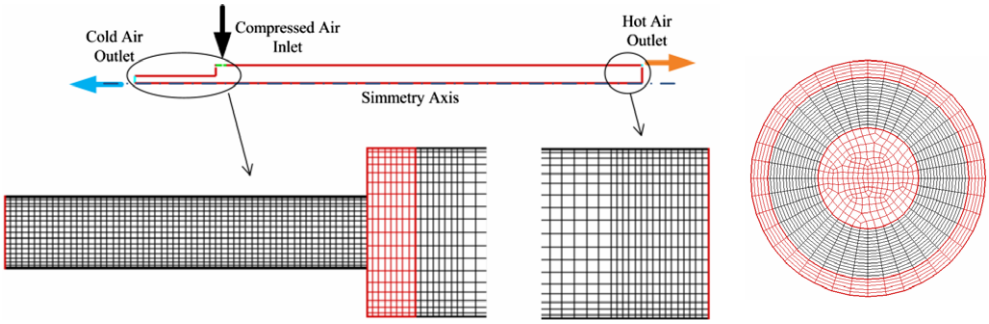

Fig. 7. Computational grid used in LES simulations.

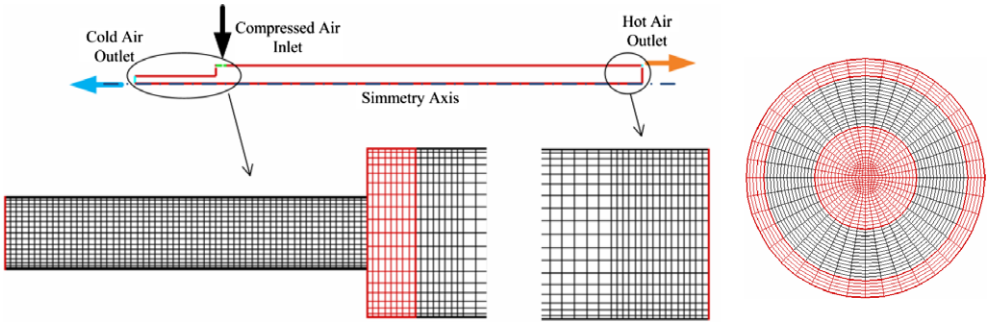

Fig. 8. Modified grid for LES simulations.

built in coupled implicit solver of the commercial finite volume code FLUENT™ 6.3.26. Boundary conditions are expressed, according to Skye et al. [1], by imposing pressure, temperature and velocity components values at the computational inlet, and pressure values at the outlets. Their values are reported in Table 4.

$$\frac{\partial \rho}{\partial t} + \frac{\partial}{\partial x_j}(\rho u_j) = 0 \tag{1}$$

$$\frac{\partial}{\partial t}(\rho u_i) + \frac{\partial}{\partial x_j}(\rho u_i u_j) = -\frac{\partial p}{\partial x_i} + \frac{\partial \tau_{ij}}{\partial x_j} \tag{2}$$

$$\frac{\partial}{\partial t}(\rho E) + \frac{\partial}{\partial x_j}[u_j(\rho E + p)] = -\frac{\partial \phi_j}{\partial x_j} + \frac{\partial}{\partial x_j}(u_i \tau_{ij}) \tag{3}$$

$$\tau_{ij} = \mu\left(\frac{\partial u_i}{\partial x_j} + \frac{\partial u_j}{\partial x_i}\right) - \frac{2}{3}\mu \frac{\partial u_k}{\partial x_k}\delta_{ij} \tag{4}$$

$$\phi_j = -\lambda \frac{\partial T}{\partial x_j} \tag{5}$$

$$p = \rho R T \tag{6}$$

No-slip and adiabatic conditions are set at the solid bounds and atmospheric pressure is imposed at both the exits. Eqs. (1)–(6) (in which any volumetric internal heat source has been neglected) with their initial and boundary conditions, represent a set of relations that describe the exact behavior of a Newtonian fluid in a laminar or turbulent regime. Anyway, in the case of turbulent solutions like in vortex tube flow, the direct numerical solution is a purely theoretical abstraction on account of it's extremely high computational costs. Hence, in the solution of high-Re flows, turbulence modelling is needed in order to obtain an accurate solution at acceptable computational costs. This approach lacks of all the details of the real flow dynamics. It replaces the fluid in turbulent motion with an "equivalent non-Newtonian one" which is described by new constitutive relations. These latter are characterised by a more regular behavior of the solution in space and time. In particular, qualitative similarities in behavior have been recognized, since long in secondary structures production, both in Newtonian turbulent flow and viscoelastic fluid laminar flow [15]. In this work both the most common approaches to turbulence modelling have been tested: namely RANS and LES. In the RANS approach different turbulence models were tested, in quest of decreasing information losses yet increasing computational cost.

Table 4
Boundary conditions.

Parameter	Value
Pressure inlet p_{in} (Pa)	700,000
Hot pressure outlet p_h (Pa)	101,325
Cold pressure outlet p_h (Pa)	101,325
Inlet temperature T_{in} (K)	298.8
Tangential velocity v_θ (m/s)	47.3
Radial velocity v_r (m/s)	9.5

3.2. RANS approach to the solution

In the RANS approach to the solution of Navier–Stokes equations one renounces to solving the details of turbulent motions and deals with the effects of the turbulence on the mean motion only. Hence, the governing equations are written for the averaged quantities. This averaging operation, called Reynolds average, can be seen as a filtering performed on the physical quantities of interest in time domain. The generic fluid dynamic variable f is decomposed into two components: $f = \bar{f} + f' : \bar{f}$ is the mean component and f' is the fluctuating component. This latter is not mathematically resolved but is generally modelled. The averaging operation has the following properties:

$$\begin{aligned} \bar{\bar{f}} &= \bar{f} \\ \overline{f'} &= 0 \end{aligned} \tag{7}$$

Moreover, in the case of compressible flows, it is useful to eliminate density turbulent fluctuations from the mean motion equation using Favre's (or mass-weighted) average $\tilde{f} = \overline{\rho f}/\bar{\rho}$. The Favre's averaged mean motion equation, for the steady case and in tensor notation, can be summarized as in (8)–(14). In these relations the over bar indicates the mean value relative to the Reynolds' averaging operation, while the prime symbol represents the turbulent fluctuation around Reynolds' averaged value. In the same way, the tilde indicates Favre's averaging and the double prime symbolizes the fluctuation around Favre's averaged value. Hence, $\overline{\tau_{ij}}$ represents the Reynolds averaged stress tensor, while $\widetilde{H}$ is Favre-averaged total enthalpy. The mean flow equations (9) and (10), highlight non-zero mean fluctuating quantities that require further modelling.

$$\frac{\partial}{\partial x_j}(\bar{\rho}\tilde{u}_i) = 0 \tag{8}$$

$$\frac{\partial}{\partial x_j}(\bar{\rho}\tilde{u}_i\tilde{u}_j) = -\frac{\partial \bar{p}}{\partial x_i} + \frac{\partial \overline{\tau_{ij}}}{\partial x_j} - \frac{\partial}{\partial x_j}\left(\bar{\rho}\widetilde{u_i'' u_j''}\right) \tag{9}$$

$$\begin{aligned} \frac{\partial}{\partial x_j}\left[\bar{\rho}\tilde{u}_j\widetilde{H}\right] = &-\frac{\partial \overline{\phi_j}}{\partial x_j} + \frac{\partial}{\partial x_j}\left(-\overline{\rho u_j'' h'} + \overline{\tau_{ij} u_i''} - \overline{\rho u_j'' \frac{1}{2} u_i'' u_i''}\right) \\ &+ \frac{\partial}{\partial x_j}\left(\tilde{u}_i\overline{\tau_{ij}} - \tilde{u}_i\bar{\rho}\widetilde{u_i'' u_j''}\right) \end{aligned} \tag{10}$$

$$\begin{aligned} \overline{\tau_{ij}} = &\left[-\frac{2}{3}\mu\left(\frac{\partial \widetilde{u_k''}}{\partial x_k}\right)\delta_{ij} + 2\mu\left(\frac{\partial \tilde{u}_j}{\partial x_i} + \frac{\partial \tilde{u}_i}{\partial x_j}\right)\right] \\ &+ \left[-\frac{2}{3}\mu\left(\frac{\partial \overline{u_k''}}{\partial x_k}\right)\delta_{ij} + 2\mu\left(\frac{\partial \overline{u_j''}}{\partial x_i} + \frac{\partial \overline{u_i''}}{\partial x_j}\right)\right] = \Sigma_{ij} + \overline{\sigma_{ij}''} \cong \Sigma_{ij} \end{aligned} \tag{11}$$

$$\widetilde{\phi_j} = -\lambda \frac{\partial \widetilde{T}}{\partial x_j} \tag{12}$$

$$\overline{p} = \overline{\rho} R \widetilde{T} \tag{13}$$

$$\widetilde{H} = \widetilde{h} + \frac{\widetilde{u_i}\widetilde{u_i}}{2} + \frac{1}{2\overline{\rho}}\overline{\rho u_i'' u_i''} \tag{14}$$

The modelling of some unclosed terms presents particular difficulties due to flow compressibility and their complete formulation is not yet achieved. Anyway, in this work, the RNG k–ε model (first order closure model) based on the Boussinesque's hypothesis, and the RSM (Reynolds Stress Model second order differential closure model) have been used [16]. In the former, according to the Boussinesque's hypothesis expressed by Eq. (15), the relation between turbulent stresses and mean speed gradient is assumed to be formally similar to the viscous stress one.

$$-\overline{\rho u_i'' u_j''} + \frac{2}{3}\overline{\rho} k \delta_{ij} = 2\mu_T \left(\frac{\partial \widetilde{u_j}}{\partial x_i} + \frac{\partial \widetilde{u_i}}{\partial x_j} - \frac{1}{3}\frac{\partial \widetilde{u_k}}{\partial x_k}\delta_{ij} \right) \tag{15}$$

Moreover, in this formulation of the well-known k–ε model, the turbulent dissipation rate transport equation is modified to improve the accuracy in the prediction of swirling flows present in RHVT.

A correction term is introduced in the ε transport equation that is a function of the strain rate tensor S_{ij} and makes the RNG model more responsive to the effect of both rapid strain and streamline curvature with respect to the standard model. Further details about these terms can be found in [16].

Being the RNG k–ε more suitable than the standard model for the prediction of high swirling flows, an intrinsic assumption is made by using a turbulent viscosity model. In fact, the components of the Reynolds stress tensor at each point and time are determined by the mean velocity gradient at the same point and time (local characteristic of the turbulence model). According to Pope [17], it can be shown that this assumption is verified only if the turbulence adjusts rapidly to the mean straining of the flow. This condition is true for simple turbulent flows (like round jet, mixing layer, boundary layer), in which the mean velocity gradient can represent the "history of mean distortion of the flow", the non-local transport processes are small and the turbulence production almost balances dissipation. In these cases the local character of the Boussinesque's hypothesis is acceptable and a turbulent viscosity model can be used. Moreover, in the first order closure models there is an explicit assumption related to the structure of Reynolds stress tensor. In fact, the Boussinesque's relation imposes the isotropy of the normal components in the turbulent stress tensor. This assumption was found to be experimentally incorrect in several classes of flows like strong swirling flows, flows with significant streamline curvature and flows in non-circular ducts (which presents secondary vortex structures). Hence, the use of closure models derived from the Boussinesque's hypothesis in high swirling flows, like the ones in RHVT, may introduce several assumption with no physical meaning. In order to avoid this, in this work a more complex turbulence model, like RSM, has been used in the RANS simulations. This closure model does not introduce unrealistic hypotheses and at the same time its results can be compared with the ones from the RNG k–ε performing a test on prediction capability of the simpler model. In the RSM model six more partial differential equations need to be solved: one additional transport equation for each component of the Reynolds stress tensor. Despite the increased computational costs, RSM is the most suitable model for studying those complex flows with high swirling and stress-induced secondary flows which are related to the anisotropy of the Reynolds stresses tensor normal component. The RSM model is therefore the natural choice since these two features are both present in the Ranque–Hilsch vortex tube flows.

The complete transport equations for Reynolds stresses are directly obtained from the momentum conservation equations, written following the RANS approach. Nevertheless, RANS and Reynolds stresses equations do not constitute a closed set system; hence, several terms require further modelling, like triple correlation, pressure–strain correlation, Reynolds stress dissipation, etc. In this work, these terms are modelled by means of linear relations between them and Reynolds stresses mean gradients [16]. Anyway convection, production and molecular diffusion of Reynolds stresses are taken into account exactly by the transport equation.

The discretization of convective terms in the mass, momentum and energy conservation equations relied on SOU (Second Order Upwind) scheme, whereas a QUICK (Quadratic Interpolation for Convective Kinematics) discretization scheme was used for the k, ε and RSM equations. In fact, high values of Reynolds cell number advise against the use of centered schemes. Frictionless flux treatment was performed by means of a Roe Flux Difference Splitting scheme with the Courant number varying from 0.5 to 5. Lower under-relaxation factors ranging from 0.05 to 0.8 were chosen for momentum, pressure, swirl velocity and turbulent dissipation rate. Convergence criterion value for all the thermo-fluid dynamic variables was fixed to 10^{-3}.

3.3. LES approach to the solution

In a turbulent motion the dimensions of the largest scale eddies are comparable to the macroscopic dimension of the flow field, while the smallest eddies, i.e. those responsible for the viscous dissipation, are in the range of the Kolmogorov scales.

When using a LES approach to the simulation of turbulent flow a spatial filter to the Navier–Stokes equations is applied in order to filtering out the smallest eddies scales and explicitly resolve the motion equations for the others. Hence, in contrast to the RANS approach, LESs resolve explicitly the motion equations for the large turbulent scales and model the effect of the smaller ones. Following the Kolmogorov theory, these latter scales are universal, i.e. their dimensions are independent from macroscopic boundary condition, and so the closure model can be universal and do not need many specific calibrations constant to adapt itself to a generic flow. Being turbulence an unsteady, three-dimensional phenomenon, problem formulation must be unsteady and three-dimensional too, so neither geometrical nor analytical simplifications are possible. In a LES the generic fluid dynamic variable f is decomposed into two components: a filtered $\bar{f}$ or resolved component and a sub-filter or sub-grid component f', not resolved or modelled (16).

$$f = \bar{f} + f' \tag{16}$$

For a compressible flow, as the RHVT one, Favre filtering is performed with the same notation as the one previously used. The filtered generic fluid dynamic variable in a compressible flow is expressed as in (17),

$$f = \tilde{f} + f'' \tag{17}$$

in which $\tilde{f} = \overline{\rho f}/\bar{\rho}$ and over bar or tilde indicate spatial filtering operations. Filtering operation can be performed either in the physical space or in the Fourier space (wave number space) depending on the filter functions G. Hence, the filtered component of f can be defined (in physical space) as follows:

$$\overline{\rho f}(\mathbf{x}, t) = \int_{\Omega \times [0,T]} \rho f(\mathbf{y}, t') G(\mathbf{x} - \mathbf{y}, t') d^3\mathbf{y}\, dt' \tag{18}$$

where G can be a function like Top-Hat Filter, Sharp Cut-Off Filter or Gaussian filter, $\mathbf{x}$ and $\mathbf{y}$ are position vectors and Ω is the computa-

tional domain. Anyway the finite volume discretization itself provides the spatial filtering operations by means of a filter function defined in (19):

$$G(\mathbf{x}-\mathbf{y}) = \begin{cases} 1/V & \mathbf{y}\epsilon V \\ 0 & \mathbf{y} \text{ otherwise} \end{cases} \tag{19}$$

where V is the volume of the computational cell. Doing so, the filter is identified with the computational grid and only eddies with dimension larger than the grid dimension are explicitly resolved, while the others are modelled. It follows that the sub-filter model is a real sub-grid one. Moreover, the finite volume discretization implies analytical simplifications in LES as the outcome of the filtering operation. Only one term of the sub-grid stress tensor, called sub-grid Reynolds stress is produced, as in time averaging of the Navier–Stokes equations (RANS).

Further details can be found in [18,19]. The LES equations implemented can be expressed in (21)–(23), in which H and ϕ_j have the same expressions as in RANS equations. This set of equations is closed by using a sub-grid closure model (Smagorinsky's one).

$$\frac{\partial \overline{\rho}}{\partial t} + \frac{\partial}{\partial x_j}(\overline{\rho}\widetilde{u}_i) = 0 \tag{20}$$

$$\frac{\partial}{\partial t}(\rho\widetilde{u}_i) + \frac{\partial}{\partial x_j}(\overline{\rho}\widetilde{u}_i\widetilde{u}_j) = -\frac{\partial \overline{p}}{\partial x_i} + \frac{\partial \overline{\tau_{ij}}}{\partial x_j} - \frac{\partial}{\partial x_j}\left(\overline{\rho}\widetilde{u_i''u_j''}\right) \tag{21}$$

$$\frac{\partial}{\partial t}(\overline{\rho}\widetilde{E}) + \frac{\partial}{\partial x_j}\left[\overline{\rho}\widetilde{u}_j\widetilde{H}\right] = -\frac{\partial \overline{\phi_j}}{\partial x_j} + \frac{\partial}{\partial x_j}\left(-\overline{\rho u_j'' h''} + \overline{\tau_{ij}u_i''} - \overline{\rho u_j'' \frac{1}{2}u_i''u_i''}\right) + \frac{\partial}{\partial x_j}\left(\widetilde{u}_i\overline{\tau}_{ij} - \widetilde{u}_i\overline{\rho}\widetilde{u_i''u_j''}\right) \tag{22}$$

$$\overline{\tau_{ij}} \cong \left[-\frac{2}{3}\mu\left(\frac{\partial \widetilde{u_k}}{\partial x_k}\right)\delta_{ij} + 2\mu\left(\frac{\partial \widetilde{u_j}}{\partial x_i} + \frac{\partial \widetilde{u_i}}{\partial x_j}\right)\right] \tag{23}$$

In order to obtain the system closure, the sub-grid stress tensor is split into an isotropic and a deviatoric part as in (24); then, following the Boussinesque's hypothesis, the deviatoric part is expressed as a linear function of the filtered strain rate deformation tensor $\widetilde{S}_{ij}$ (25). Turbulent viscosity, which is a proportionality factor is expressed by Eq. (26)

$$\tau_{ij_{SGS}} = -\overline{\rho}\widetilde{u_i''u_j''} = -\overline{\rho}\left(\widetilde{u_i''u_j''} - \frac{1}{3}\widetilde{u_k''u_k''}\delta_{ij}\right) + \frac{1}{3}\overline{\rho}\widetilde{u_k''u_k''}\delta_{ij} = \tau^d_{ij_{SGS}} + \tau^i_{ij_{SGS}} \tag{24}$$

$$\tau^d_{ij_{SGS}} = -\overline{\rho}\left(\widetilde{u_i''u_j''} - \frac{1}{3}\widetilde{u_k''u_k''}\delta_{ij}\right) = 2\mu_T\left(\frac{\partial \widetilde{u_j}}{\partial x_i} + \frac{\partial \widetilde{u_i}}{\partial x_j} - \frac{1}{3}\frac{\partial \widetilde{u_k}}{\partial x_k}\delta_{ij}\right) = 2\mu_T\left(\widetilde{S_{ij}} - \frac{1}{3}\widetilde{S_{kk}}\delta_{ij}\right) \tag{25}$$

$$\mu_T = \overline{\rho}C_R\overline{\Delta}(\widetilde{S_{ij}}\cdot\widetilde{S_{ij}}) \tag{26}$$

The constant C_R is called Smagorinsky's constant; its value is 0, 1 and is experimentally determined. $\overline{\Delta}$ is the filtering length, equal to the grid dimension related to the cubic root of the mean cell volume. The isotropic part of the sub-grid stress tensor, modelled as in [20], is expressed by means of the sub-grid turbulent kinetic energy k_{SGS} and the sub-grid turbulent Mach number M_{SGS} [21]. An analogous modelling technique is used for specific sub-grid thermal flux, defined by the following expression:

$$q_j'' = -\overline{\rho}c_p\widetilde{u_j''T''} \tag{27}$$

In fact, according to the Smagorinsky's model for turbulent viscosity (26), the above equation can be written as:

$$q_j'' = -\frac{\overline{\rho}c_p}{\mathrm{Pr}_T}C_R\overline{\Delta}(\overline{S_{ij}}\cdot\overline{S_{ij}})\frac{\partial \widetilde{T}}{\partial x_j} \tag{28}$$

Simulation time step length Δt in LESs is related to the Kolmogorov time scale t_η. Its value, 49.2×10^{-6} s, was determined by means of Kolmogorov's relation [17] an integration time step was selected as a fraction it. Due to high computation time, a physical simulation interval of 20 ms was used in LES. Discretization scheme used for convective terms was a SOU scheme while time integration was performed with a second order accurate implicit scheme. Frictionless flux treatment was performed by means of a Roe Flux Difference Splitting scheme with a Courant number fixed to 1; convergence criterion value for all the thermo-fluid dynamic variable in each time step was fixed to 10^{-3}.

4. Simulation results and discussion

Simulations results are shown in Figs. 9–11. In these figures, RANS radial velocity and temperature profiles at different distances from the hot exit, varying from 2.5 mm to 70 mm (section near the inlet), are reported. They are some samples of the results obtained by using different closure models. These profiles are compared with the LES ones obtained by means of the Smagorinsky sub-grid model. Radial profiles calculated using RNG k–ε and RSM models for turbulence closures are compared with the ones obtained with the mixing length model too. Although this model is useless in describing turbulent complex flows, results obtained in this case represent the output of the simulation in the limit of the computational cost tending to zero.

In Figs. 15–17 computational models of the RHVT with axial hot outlet and with radial hot exit are compared using RANS simulations.

4.1. Turbulence model effect and comparison with LES data

RANS and LES simulations were performed on the same workstation equipped with Intel® Core™2 Quad Q6600 2.4 GHz processor. Computational time in RANS simulation, quite independent of turbulent closure models used, was about 1.5–2 h. Being LES an unsteady simulation technique, its results compared with the RANS ones were obtained by means of a time averaging operation performed over the results of each time step. Time steps considered in this operation were those needed for steady conditions, measured by the integral value of static pressure over a cross-section of the tube (Fig. 12), to be reached. The physical time interval length simulated was about 20 ms with a time step extension of 5 μs resulting in a CPU time of about 26 days.

Swirl axial and radial velocity profiles were analysed and the simulations confirmed that swirl component is the most important one being the axial velocity about an order of magnitude smaller and the radial velocity almost negligible.

The analysis of swirl velocity profiles (Fig. 9), in the case of simulation performed with RNG k–ε model, shows a nearly linear profile far from the wall regions.

Hence, simulations with RNG k–ε turbulence model show a swirl velocity profile very similar to the rigid body rotation ones. This is verified for all the sections reported except for the one near the inlet at $z = 70$ mm, in which the swirl velocity profile is substantially imposed by the inlet condition. As a result of the no-slip condition at the wall, a maximum appears near the internal surface of the tube in all sections analysed. The value of the tangential velocity on the tube axis is not exactly null, as request by symmetry: this is probably due to the numerical diffusion error that becomes more important, with upwind schemes, when convective velocity is low. These results are in agreement with [8], a previous

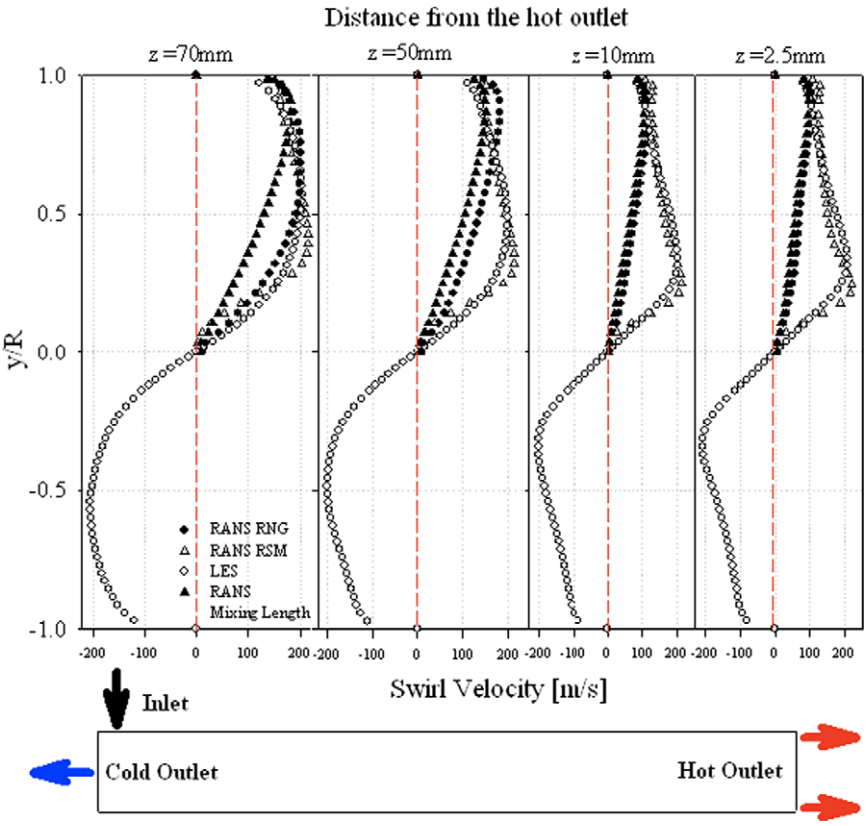

Fig. 9. Swirl velocity profiles in RANS and LES simulations at different sections.

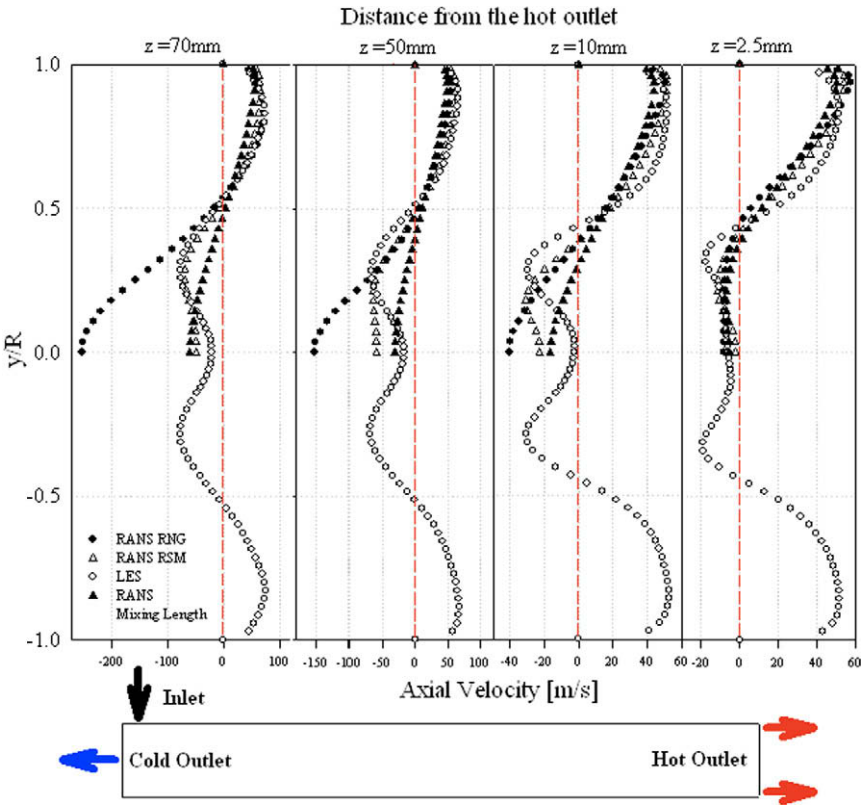

Fig. 10. Axial velocity profiles in RANS and LES simulations at different sections.

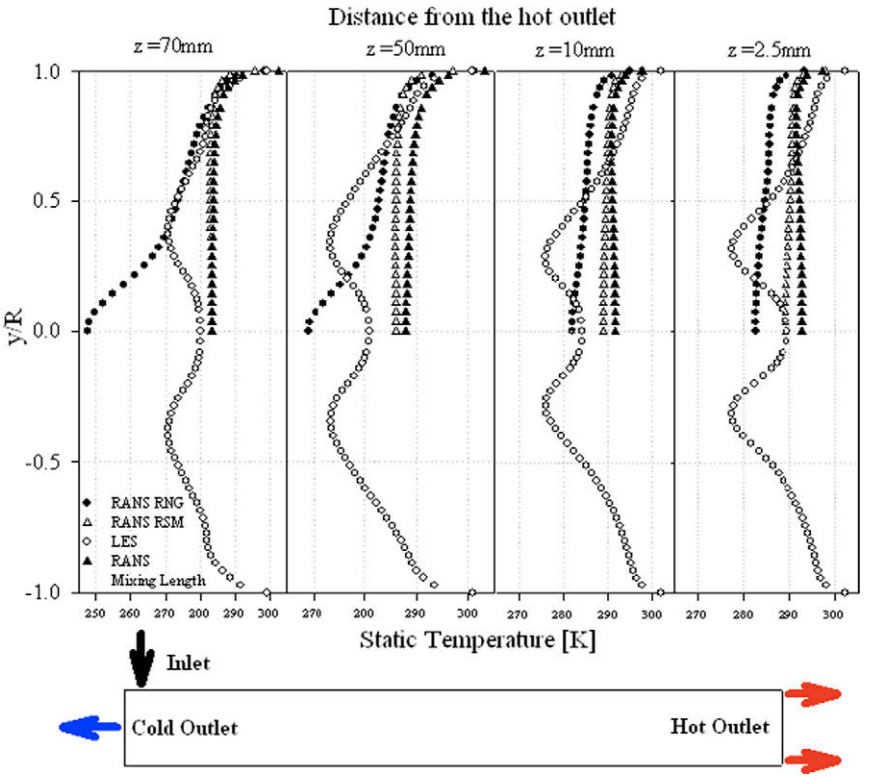

Fig. 11. Static temperature profiles in RANS and LES simulations at different sections.

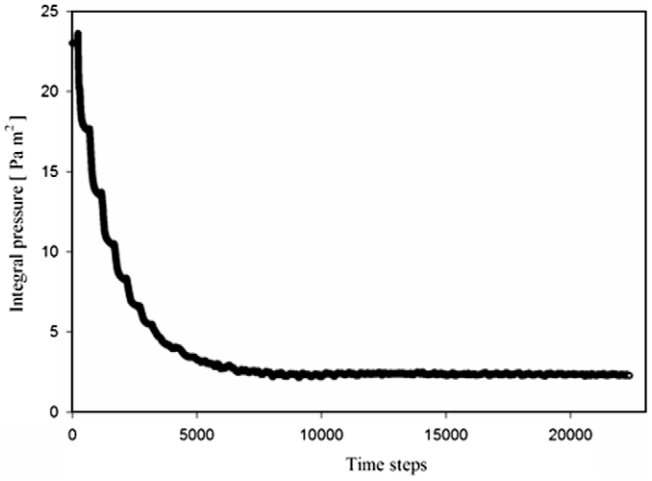

Fig. 12. Integral pressure value versus number of time step in a LES simulation (time step length 0.5 μs).

work in which the same turbulence closure was used with a RHVT having different geometrical characteristics.

Some differences can be noted comparing the results obtained by the simulation performed with non-Boussinesque turbulence models, like RSM, to data obtained with the RNG k–ε model; in particular, tangential velocity profiles at the same axial coordinate along the tube axis are fairly different. Using the RSM model, a steeper growth in the swirl velocity moving away from the axis and a smoother decreasing, moving toward the wall, are showed. This happens at all sections but near the inlet where all profiles almost collapse on the same curve. This is probably due to the influence of the inlet condition. Tangential velocity profiles obtained by the RANS simulations with RSM model show a very good agreement with the LES ones. On the other hand, RANS results, obtained with RNG k–ε and mixing length models (Boussinesque models), show strong differences (except near the inlet) with respect to the LES results.

Axial velocity profiles (Fig. 10) show a substantial difference between RNG k–ε and RSM calculations too. This discrepancy is more evident in the sections near the inlet but decreases moving toward the hot exit. Moreover, when comparing the RANS results with the LES ones, only RSM calculation demonstrate a good agreement with LES data which are the ones that seem more representative of high swirl flow axial velocity profiles. In the section near the hot outlet, swirl number decreases hence axial velocity profiles obtained from all models almost collapse on to the same curve. Anyway only RSM and LES profiles show a maximum of axial velocity far from the axis of the tube.

Strong differences between RANS and LES results can be underlined in the analysis of the static temperature profiles. In fact, RANS results show a temperature increase with the distance from the tube axis entirely located near the walls in the sections near the hot outlet. In the sections near the inlet RNG, temperature distribution present a minimum on the axis at a value far from the previous literature results, while RSM results show a flat temperature distribution and hence a more realistic static temperature value on the axis. However, LES results present temperature profiles, with a minimum far from the axis in every section with a maximum difference between the static temperature values increasing toward the cold exit.

Analysis of Figs. 9–11 shows that the choice of turbulence model strongly influences the prediction of the velocity and the temperature fields by means of RANS simulations. Moreover, in the simulation of velocity profiles, results obtained by using the RSM model are closer to LES results, with respect to the RNG data. On

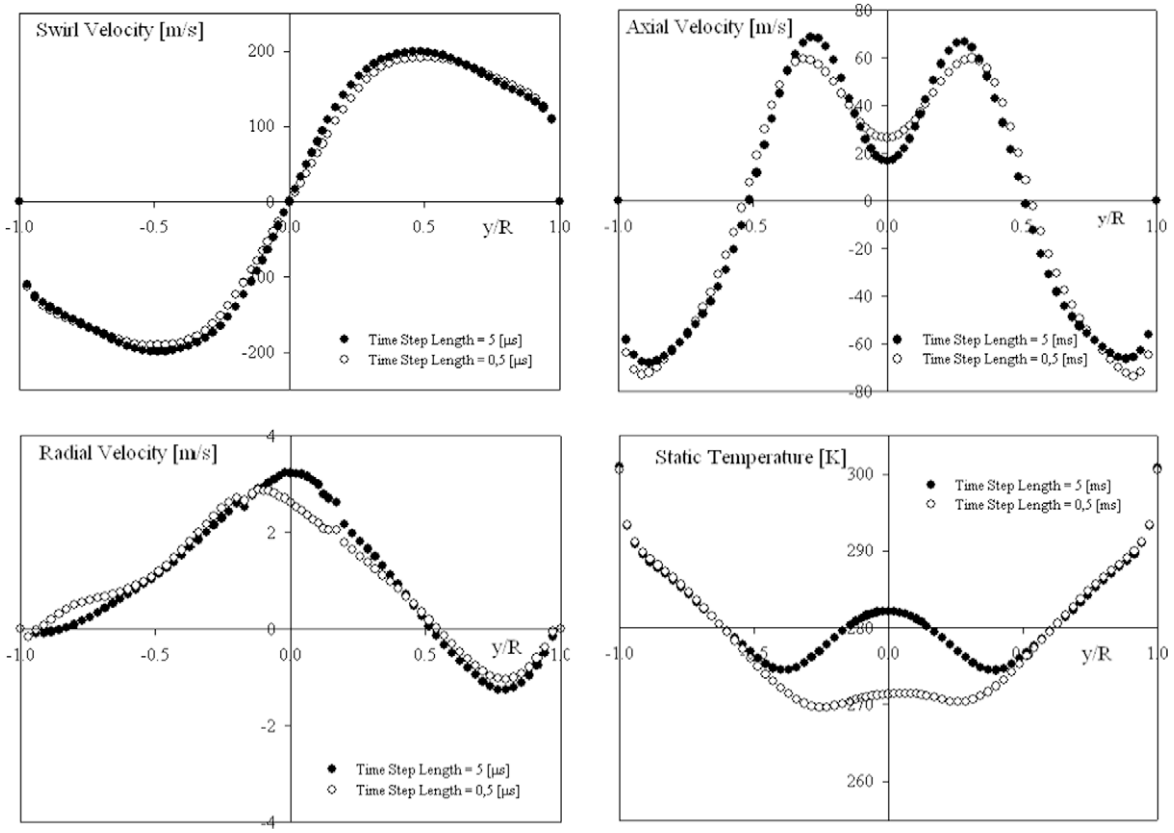

Fig. 13. Velocity and static temperature profiles in LES varying time step length (5 μs, black dots; 0.5 μs, white dots; section at $z = 50$ mm; $x = 0$ mm).

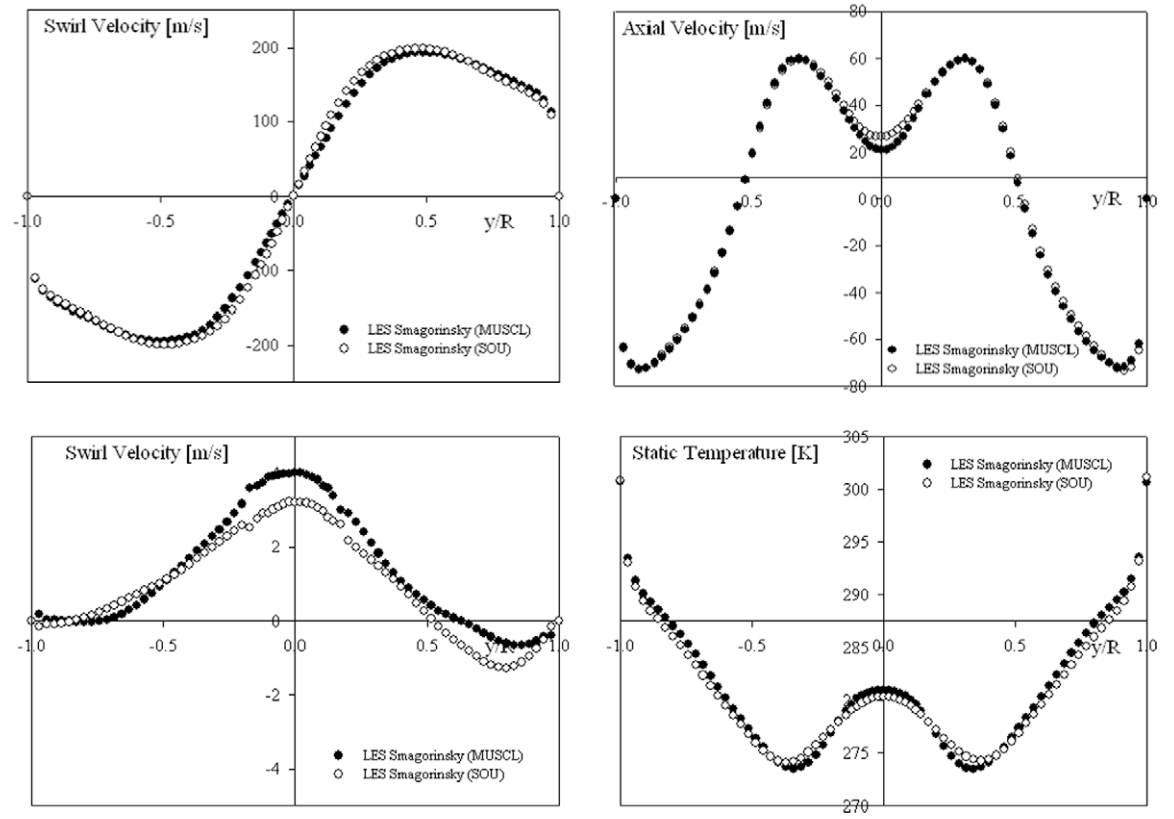

Fig. 14. Velocity and static temperature profiles in LES varying discretisation scheme (third-order MUSCL, black dots, SOU, white dots; section at $z = 50$ mm; $x = 0$ mm).

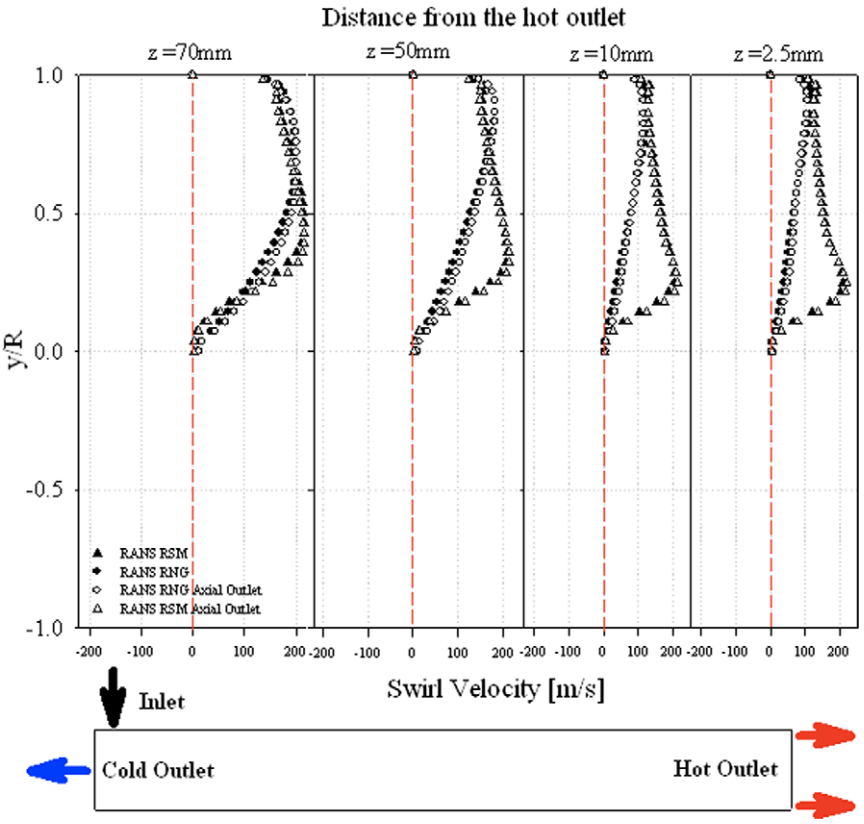

Fig. 15. Swirl velocity profiles in RANS simulations on computational models with radial and axial hot outlet (at different sections).

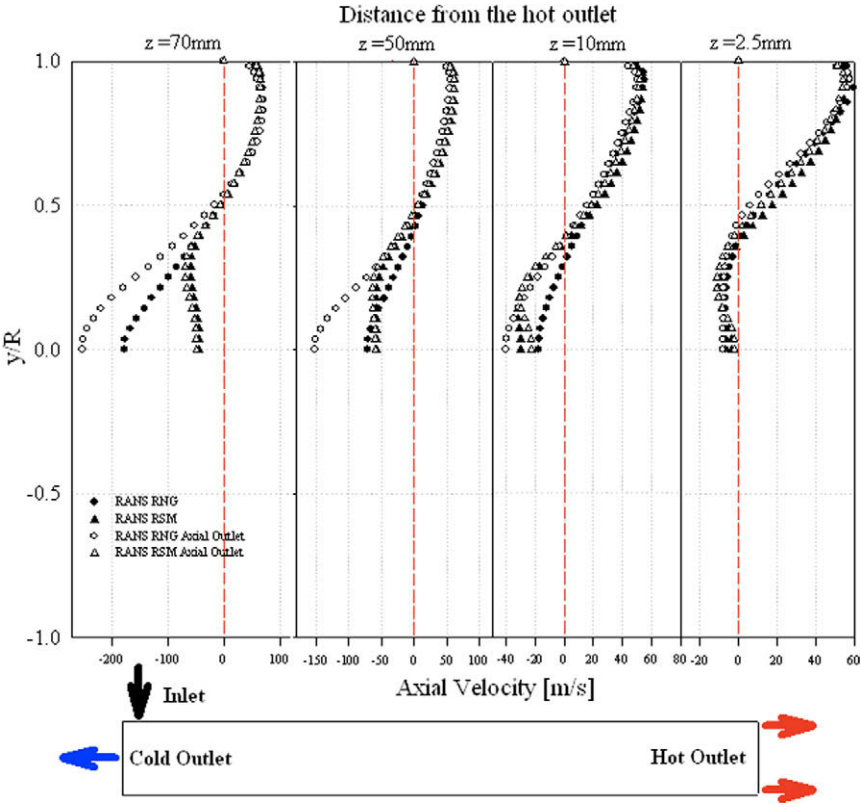

Fig. 16. Axial velocity profiles in RANS simulations on computational models with radial and axial hot outlet (at different sections).

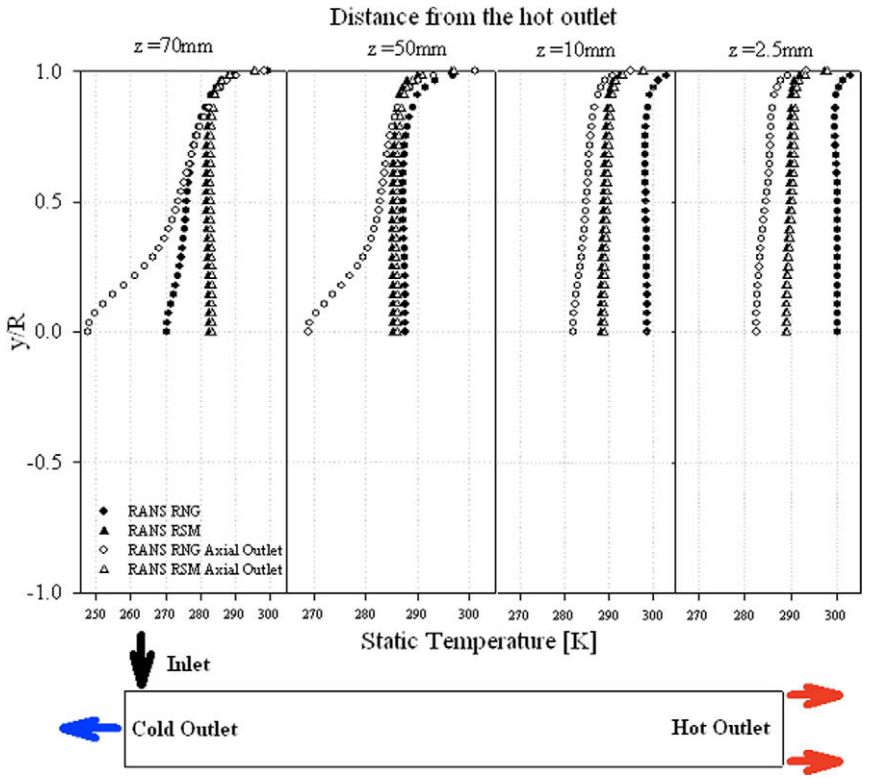

Fig. 17. Static temperature profiles in RANS simulations on computational models with radial and axial hot outlet (at different sections).

the other hand, static temperature profiles in RANS simulations are not much influenced by the turbulence model (far from the inlet) and are far from LES previsions. In fact, LES profile of static temperature, in each section of the tube considered, show a value on the axis higher than in the surroundings, which is not enlightened by RANS simulations. This behavior could be interpreted considering that LES simulations reveal values of the axial and the tangential velocity on the axis lower than in the surroundings. This results in lower values of the kinetic energy on the axis and hence higher values of static temperature.

In the assessment analysis of time averaged LES results, an asymmetric profile of radial velocity was noted (lower left plot of Fig. 13 for $z = 50$ mm). That could be imputed to the choice of a too short averaging time; in fact, being radial speed the lower velocity component, it would have needed a higher averaging time to reach a steady condition. Nevertheless, the importance of radial velocity in the fluid dynamic behavior of the RHVT and in the thermal separation phenomenon is negligible, as confirmed by recent numerical results too [8]. To investigate time step length influence on LES results a further large eddy simulation, with the same set-up of the previously described one, but with a time step length 10 times lower (equal to 0.5 μs), was conducted. The results obtained by this simulation (showed in Fig. 13 by white dots) revealed a dependency of the radial velocity and the static temperature profiles from the time step length, while tangential and axial velocity seemed to be poorly affected by the time step length variations. A longer simulation time, at the moment incompatible with the computing resources available, could probably remove this dependency. Moreover, numerical diffusion due to discretization was considered as another potential source of this discrepancy. At this point further analysis was performed by means of a LES with a low-diffusion discretization method (third-order MUSCL [15]). Results of the "low-diffusion LES" (Fig. 14) seem to reveal very little influence of the discretization scheme on the swirl velocity, the axial velocity and the temperature profiles while more evident effects can be underlined on the radial velocity.

It can be concluded that the RANS RSM simulations demonstrate better agreement in the prediction of velocity field with respect to the RNG ones when compared with LES results, regardless a computational cost not much higher in our simulations. This result seems to confirm that in complex flows, such as those taking place in a Ranque–Hilsch vortex tube (in which the main features are the result of the anisotropy of Reynolds stresses tensor normal component), the choice of RSM as turbulence model is more suitable. Nevertheless, when predicting the temperature field inside the tube, RANS simulations show results quite different from the LES ones, with any of the turbulence models tested.

4.2. Effect of the computational model hot outlet

In order to avoid further simplifications in the computational domain an axial hot outlet was used in all the simulations performed during this work. Axial hot outlet was considered to be more realistic since it is closer to the condition in which RHVT operates as a jet impingement cooler. Anyway, several numerical studies are present in the literature, using a computational radial hot outlet [1,10,22] hence an investigation on the influence of this computational model feature was conducted using RANS simulations.

Flow field simulations were performed on a computational model having a radial hot outlet and the same initial and boundary conditions previously described.

A comparison of the results are reported in Figs. 15–17, in which swirl velocity, axial velocity and static temperature radial profiles are plotted for RANS RNG and RSM simulations. These were performed on the model with an axial hot outlet and on the model with the radial one. The analysis underlines that RANS results with RSM are almost unaffected by the variation of the outlet in the computational model. In the RNG simulations the influ-

ence of the hot outlet model used is particularly evident on axial velocity and temperature profile especially in the sections located near the inlet (z = 70 mm and z = 50 mm). Moreover, neither increment of the computational costs nor stability problems in the solution were found in simulations when varying the hot outlet feature. This could confirms that a computational model with an axial hot outlet, which is closer to real condition of the vortex tube in jet impingement operation, is effective in the RHVT internal flow RANS simulations, in particular when coupled with a RSM turbulence model.

5. Conclusion

The aim of this work was to perform an accurate numerical analysis of a Ranque–Hilsch vortex tube (RHVT) internal flow in jet impingement operation. Commercial CFD code FLUENT™ 6.3.26 was used to perform numerical simulations of the flow pattern inside the device. The CFD simulation of the flow field in a Ranque–Hilsch vortex tube is a challenging task because of its compressibility, turbulence and high swirl. Moreover, experimental measurement of the internal velocity and temperature fields necessary for the verification are, in author's opinion, very difficult to obtain. Hence, several different approaches to the simulation of the turbulence (RANS and LES) were tested. Furthermore, different turbulence models were used as RANS equations closures: RNG k–ε model and a linear RSM (differential Reynolds Stress Model). Convergence, in a simulation of RHVT internal flow, was obtained for the first time with an RSM closure. Large Eddy Simulations of the internal flow, using the Smagorinsky's sub-grid model, were performed too and a grid independence procedure, by means of Richardson extrapolation, was conducted on both RANS and LES simulations, showing that results were independent of grid spacing used, in both approaches. Calculations were performed on computational model of a commercial RHVT analysed in previous works [1], with an axial computational hot outlet, closer to the real behavior of the device in jet impingement cooling operation. Another example of RHVT internal flow LES exists in the literature (Farouk and Farouk [22]) but it was performed on a computational model with a radial hot exit.

RANS simulations were performed on an axial-symmetric computational domain, while LES were performed on a (complete) three-dimensional computational model in order to avoid symmetry imposing in turbulent structures.

Results showed that flow in the tube is split into two helical coaxial streams, with different thermal features, placed near the internal wall of the tube, the hot one, and near the axis, the cold one. A sketch of instantaneous streamlines patterns obtained by LES is showed in Fig. 18. Static temperature values are represented by colour bands: double co-rotating helical flow patterns are enlightened.

Flow patterns and velocity profiles in different sections of the tube show a qualitative good agreement with the results available by previous works. Strong differences between results obtained by RANS RNG k–ε and RSM closures are showed in the axial velocity profiles, far from the hot outlet and in the swirl velocity profiles, far from the inlet. This result could be expected as turbulence closures features. Simulation with RSM model predicts an axial velocity profile, close to a fully developed channel flow one, while LES shows a "camel's hump" trend for axial velocity profile. LES and RANS simulations, in the version with RSM model, are able to predict a velocity profile similar to a "Rankine Vortex" one for the swirl velocity component. All the simulations confirmed that radial velocity values are very small when compared with axial and tangential ones; hence, this component could be ignored in the analysis of the thermal separation process as in a recent numerical works [8]. RANS simulations proved capable of predicting secondary circulation flow inside a RHVT although this approach showed a single re-circulating vortex structure that extends all over along the tube length. LES can simulate secondary circulation flow too; anyway a more complex secondary vortex structure appears in this case, due to the three-dimensional and unsteady features of the flow field. Numerous secondary vortex take place along the tube length (Fig. 19), yet smaller than in the RANS case. Instantaneous flow field predicted by LES is non-symmetric and, only averaging LES results on time, an axis-symmetric flow field can be obtained. The mechanism of vortex formation and break-down at the interface between the two co-axial streams is similar to the Kelvin–Helmholtz instability.

In the prediction of the temperature field, RANS models show radial temperature profiles very close between them far from the inlet, while LES predicts a lower temperature near the tube axis and a considerably different static temperature radial profile. Temperature radial profiles demonstrate a qualitative good agreement with data by previous works.

The influence of the computational model used, was evaluated comparing numerical results obtained by RANS simulation in the case of axial and radial hot outlet. Simulations demonstrate that RSM previsions are unaffected by the computational hot outlet variation, while in RNG results some effects can be underlined in axial velocity and temperature profiles, particularly near the inlet.

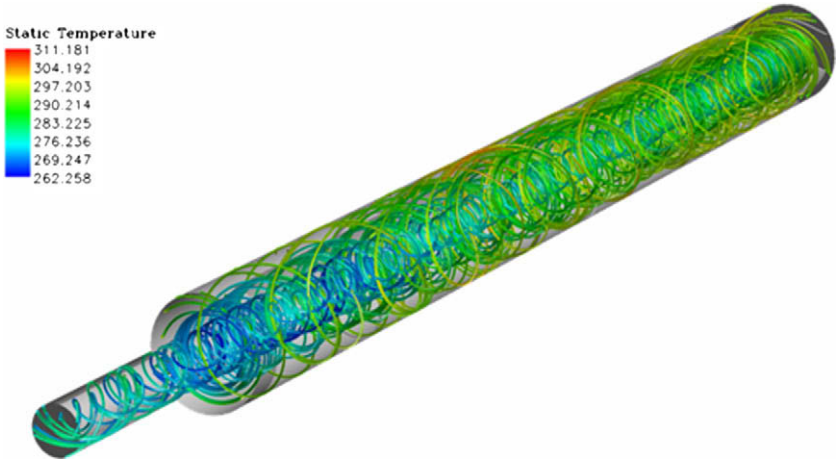

Fig. 18. Three-dimensional visualization of streamlines patterns with temperature map, obtained by LES with Smagorinsky closure model.

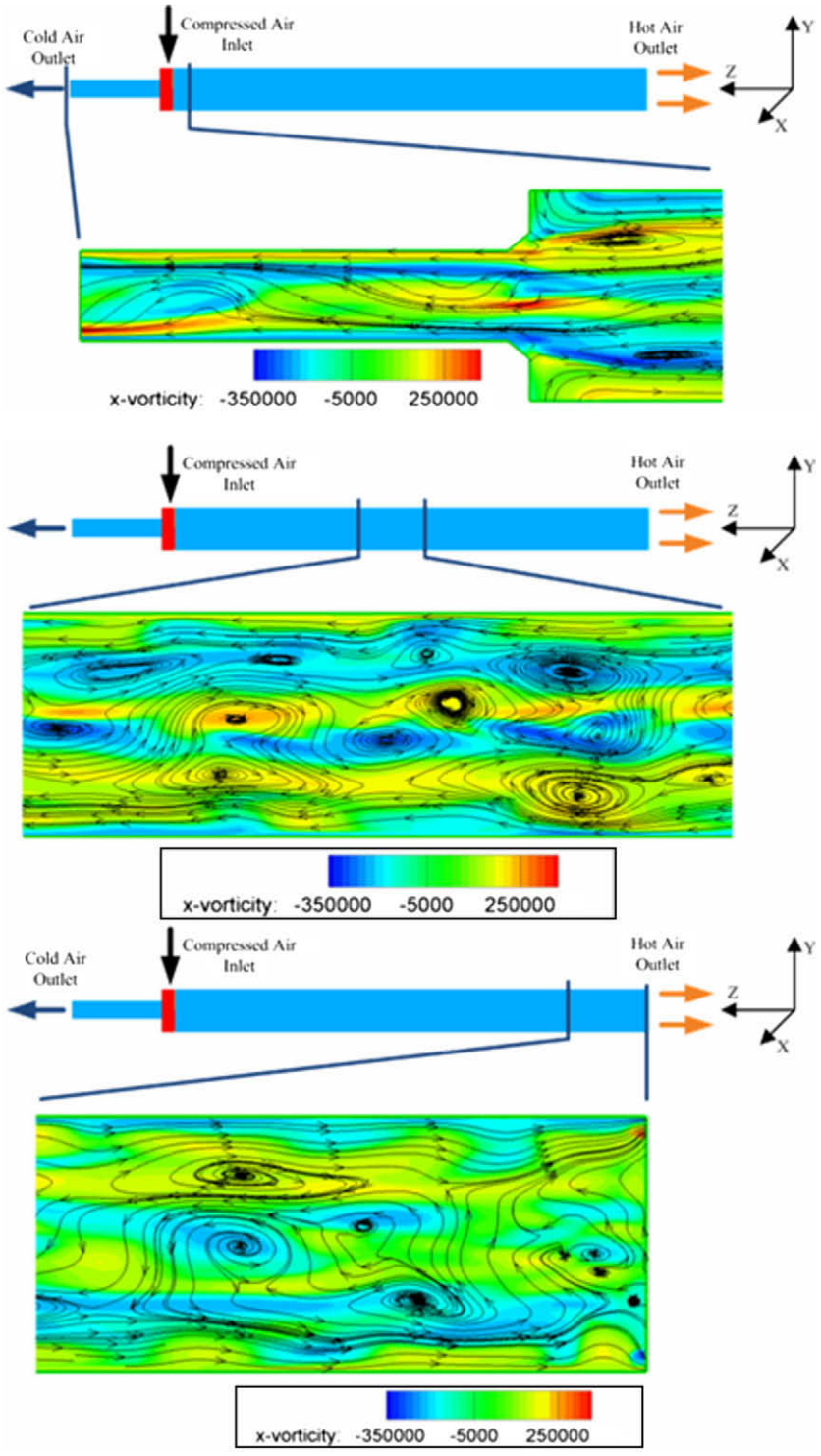

Fig. 19. *X*-vorticity maps with streamlines patterns superimposed, obtained by LES.

An accurate estimation of errors in the simulations was performed and those due to skewness and cells misalignment were reduced by finely tuning the grid type that had to be used. Time step influence was evaluated performing two LES with different time step extensions. This analysis enlightened that radial velocity and temperature prevision are influenced and that only longer lasting simulation time could improve the accuracy of the evaluation. Results of a "low-diffusion LES" performed using a low-diffusion discretization scheme seems to confirm the small relevance of this kind of error particularly in the prediction of temperature, swirl and axial velocity components.

The results obtained by CFD can be used when modelling boundary conditions in the numerical simulations of outgoing jets. This way important information needed for the estimation of jet impingement capability of the device would be available. Moreover, a CFD analysis focused on velocity and temperature fields

scaling with vortex tube dimensions could improve the potential of experimental verification of the internal flow field numerical prevision.

References

[1] H.M. Skye, G.F. Nellis, S.A. Klein, Comparison of CFD analysis to empirical data in a commercial vortex tube, Int. J. Refrig. 29 (2006) 71–80.
[2] R.T. Balmer, Pressure-driven Ranque–Hilsch temperature separation in liquids, J. Fluids Eng. 110 (1988) 161–164.
[3] M. Kurosaka, Acoustic streaming in swirling flows and the Ranque–Hilsch (vortex tube) effect, J. Fluid Mech. 124 (1982) 139–172.
[4] B.K. Ahlborn, S. Groves, Secondary flow in a vortex tube, Fluid Dyn. Res. 21 (1997) 73–86.
[5] B.K. Ahlborn, J.M. Gordon, The vortex tube as a classic thermodynamic refrigeration cycle, J. Appl. Phys. 88 (6) (2000) 3645–3653.
[6] C.M. Gao, Experimental study on the Ranque–Hilsch vortex tube, Ph.D. Thesis, Technisce Universiteit Eindhoven, Holland, 2005.
[7] C.M. Gao, K.J. Bosschart, J.C.H. Zeegers, A.T.A.M. de Waele, Experimental study on a simple Ranque–Hilsch vortex tube, Cryogenics 45 (2005) 173–183.
[8] U. Behera, P.J. Paul, K. Dinesh, S. Jacob, Numerical Investigation on flow behavior and energy separation in Ranque–Hilsch vortex tube, Int. J. Heat Mass Transfer (2008).
[9] S. Eiamsa-ard, P. Promvonge, Review of Ranque–Hilsch effect in vortex tubes, Renew. Sust. Energy Rev. 12 (2008) 1822–1842.
[10] N.F. Aljuwayhel, G.F. Nellis, S.A. Klein, Parametric and Internal study of the vortex tube using a CFD model, Int. J. Refrig. 28 (3) (2005) 442–450.
[11] S. Eiamsa-ard, P. Promvonge, Numerical investigation of the thermal separation in a Ranque–Hilsch vortex tube, Int. J. Heat Mass Transfer 50 (2007) 821–832.
[12] S. Eiamsa-ard, P. Promvonge, Numerical prediction of the vortex flow and thermal separation in a subsonic vortex tube, J. Zejiang Univ. Sci. A 7 (8) (2006) 1406–1415.
[13] U. Behera et al., CFD analysis and experimental investigations towards optimizing the parameters of Ranque–Hilsch vortex tube, Int. J. Heat Mass Transfer 48 (2005) 1961–1973.
[14] P.J. Roache, Verification and Validation in Computational Science and Engineering, Hermosa Publishers, 1998, ISBN 0913478083.
[15] C.G. Speziale, On non-linear *K–e* and *K–l* models of turbulence, J. Fluid Mech. 178 (1987) 459–475.
[16] Fluent User's Guide, release 6.3.26, Ansys Inc. USA, 2006.
[17] S.B. Pope, Turbulent Flows, Cambridge University Press, Cambridge, 2000, ISBN 0521598869.
[18] G. Comini et al., Fondamenti di Termofluidodinamica Computazionale, second ed., SGE Editoriali Padova, Italy, 2004, ISBN 8886281889.
[19] P. Sagaut, Large Eddy Simulation for Incompressible Flows, Springer, Berlin, 2002, ISBN 3540437533.
[20] Yoshizawa, Statistical theory for compressible turbulent shear flows, with the application to subgrid modelling, Phys. Fluids (29) (1986) 2152–2164.
[21] G. Erlebacher, M.Y. Hussaini, C.G. Speziale, T.A. Zang, Toward the large-eddy simulation of compressible turbulent flows, J. Fluid Mech. 238 (1992) 155–185.
[22] T. Farouk, B. Farouk, Large eddy simulation s of the flow field and temperature separation in the Ranque–Hilsch vortex tube, Int. J. Heat Mass Transfer 50 (2007) 4724–4735.